

# Dissipation induced transitions in elastic strings

Michael Nguyen<sup>1,2</sup>, Suriyanarayanan Vaikuntanathan<sup>1,2</sup>

<sup>1</sup>The James Franck Institute, The University of Chicago, Chicago, IL, and

<sup>2</sup> Department of Chemistry, The University of Chicago, Chicago, IL.

Stochastic thermodynamics provides a useful set of tools to analyze and constrain the behavior of far from equilibrium systems. In this paper, we report an application of ideas from stochastic thermodynamics to the problem of membrane growth. Non-equilibrium forcing of the membrane can cause it to buckle and undergo a morphological transformation. We show how ideas from stochastic thermodynamics, in particular a recent application to self-assembly, can be used to phenomenologically describe and constrain morphological changes excited during a non-equilibrium growth process.

Non-equilibrium forces can potentially provide new routes to modulate self-assembly and organization [1–4]. In biophysical contexts, it has been established that non-equilibrium forces play a crucial role in suppressing rogue fluctuations and enhancing fidelity of molecular recognition [3, 5–8], support robust oscillations crucial for the maintenance of circadian rhythms [9], and drive sensory adaptation processes [2, 3]. Non-equilibrium forces also play an important role in modulating cell shape and cell membrane fluctuations [10, 11]. For instance, local changes in surface tension or lateral pressure due to a spontaneous assembly of membrane proteins has been known to induce instabilities in membrane fluctuations [12–15]. Such instabilities have been implicated as important precursors during cell division [10]. Non-equilibrium fluctuations are also important in cases where the cell membrane interacts with growing actin filaments. The important role played by such interactions in regulating the organization of the membrane has been well established [16, 17].

Unlike the behavior and characteristics of equilibrium systems, where no energy is dissipated, general principles governing fluctuations about a steady state or the steady state itself in far-from-equilibrium conditions are just being discovered. In particular, the field of stochastic thermodynamics has provided a promising framework to study non-equilibrium systems in mesoscopic scale [18]. The ideas of stochastic thermodynamics have been productively used to elucidate tradeoffs between energy consumption and organization in biochemical reaction networks [7–9], self-propelled or driven colloids [19–21], and molecular motors [22, 23]. Previously, we have also shown how stochastic thermodynamics can be used to derive general design principles for self-assembly [24].

In this letter, we use the framework of stochastic thermodynamics to investigate non-equilibrium growth and morphological changes in a model elastic membrane [25–29]. Our model consists of two-dimensional particles connected by elastic springs in a ring geometry (Fig 1). The interactions between particles are chosen such that the fluctuations of the ring at equilibrium can be described by specifying a surface or a line tension and a bending

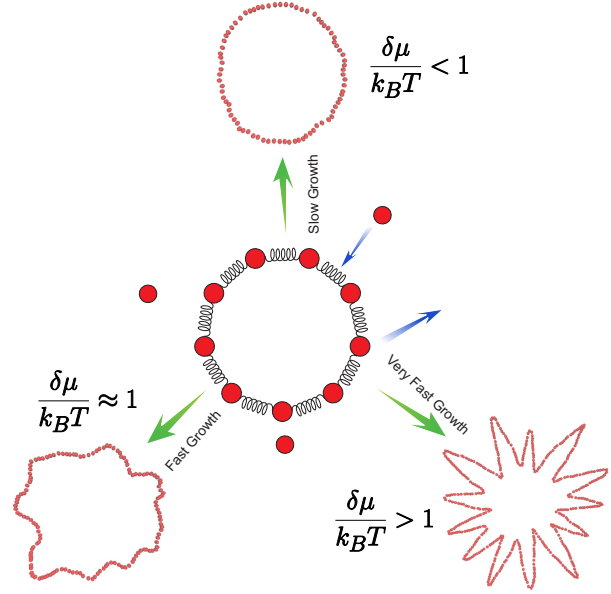


FIG. 1. Schematic of the growing assembly. When the assembly grows slowly, its shape remains circular (top figure). As the assembly grows faster, its shape becomes more distorted (lower left) and ultimately it buckles into a star-shaped morphology (lower right).

rigidity. The ring assembly is allowed to exchange particles with a reservoir. The chemical potential of the reservoir controls the growth rate of the ring assembly and sets the non-equilibrium driving force in this system.

Despite its apparent simplicity, this elastic model possesses many features [26–31] characteristic of three-dimensional membranes and can be used to obtain insights into how morphological changes in such systems can be excited under a non-equilibrium driving force. Indeed, as we describe below, our numerical analysis shows that the effective surface tension and bending rigidity of the elastic ring get modified under non-equilibrium growth conditions. Further, beyond a critical chemical potential driving force, the effective surface tension of the elastic ring is renormalized to zero and the elastic ring exhibits a buckling instability and undergoes a non-

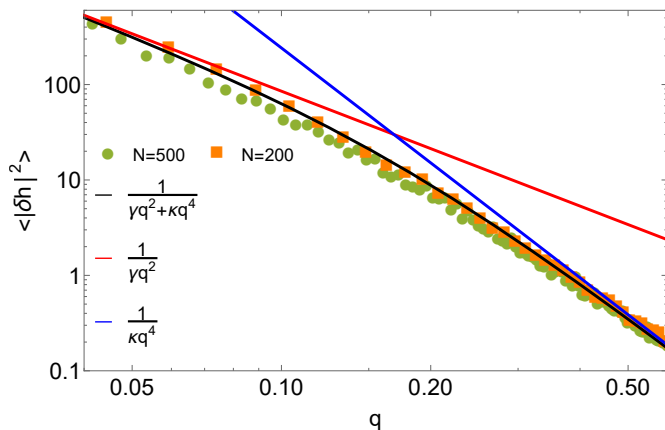


FIG. 2. Power spectrum of interfacial fluctuations at equilibrium. For small wavevectors,  $q$ ,  $|\delta h(q)|^2 \propto q^{-2}$  while  $|\delta h(q)|^2 \propto q^{-4}$  at high  $q$  in agreement with expectations Eq. 3. The data here is for  $k_s = 4$  and  $k_\theta = 6$ .

equilibrium morphological transformation (Fig 1). Such instabilities have been observed in experiments investigating the growth of model lipid membranes [28].

Using ideas from stochastic thermodynamics, we provide a phenomenological thermodynamic prescription for how the surface tension and bending rigidity are modified by the non-equilibrium forces (Eqs. 7 and 8). The phenomenological thermodynamic prescription only requires information about the magnitude of the non-equilibrium chemical potential driving force, the equilibrium surface tension and bending rigidity, the average rate of growth, and fluctuations in the average rate of growth. This thermodynamic prescription was first developed by us in [24] in the context of different self-assembly problems and is otherwise insensitive to any of the kinetic details used in the growth process. This phenomenological thermodynamic theory provides bounds on the energetic requirements to induce morphological transformations such as the above described non-equilibrium buckling transition (Fig. 6). We now describe the specifics of the elastic model, phenomenology observed in the non-equilibrium growth process, and how an application of ideas from stochastic thermodynamics can explain this phenomenology.

Our specific model consists of particles in a ring like geometry interacting according to the following Hamiltonian,

$$E = \frac{k_s}{2}(l - l_0)^2 + k_\theta(\theta - \pi)^2, \quad (1)$$

where  $l$  is the distance between neighboring particles,  $l_0$  is the equilibrium distance and  $\theta$  is the angle that neighboring particles make. The growth dynamics were simulated using the following rules. Particles are added to the elastic ring with the probability  $\min\{1, e^{(-\Delta E + \mu)/k_B T}\}$  while attempts to remove particles

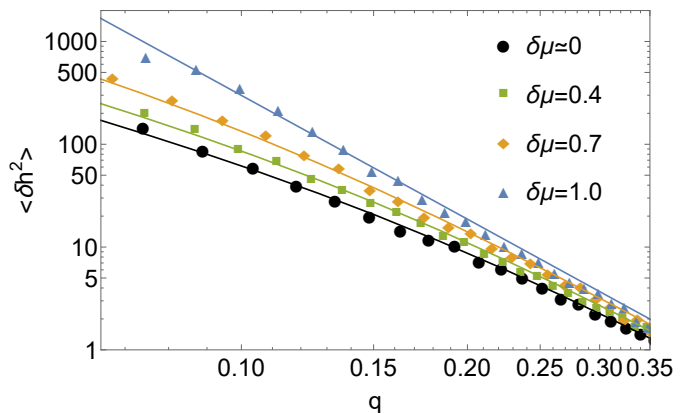


FIG. 3. Power spectrum of interfacial fluctuations at different  $\delta\mu$ . Fitting these curves to Eq. 3 allows to obtain estimates of  $\gamma_{\text{eff}}$  and  $\kappa_{\text{eff}}$  as described in the text. This analysis reveals that  $\gamma_{\text{eff}}$  decreases with increasing  $\delta\mu$ . The data here is for  $k_s = 4$  and  $k_\theta = 6$ .

from the assembly are accepted according to the probability  $\min\{1, e^{(-\Delta E - \mu)/k_B T}\}$ . Here,  $\mu$  is a chemical potential and  $k_B T$  sets an energy scale.

The rate of growth of the elastic assembly can be tuned by varying  $\mu$ . Specifically, for values of  $\mu$  above a *co-existence* value  $\mu_{eq}$ , the elastic ring polymer starts to grow. When  $\delta\mu/k_B T \equiv (\mu - \mu_{eq})/k_B T$  is small, the elastic assembly grows slowly and roughly retains its circular shape. With increasing  $\delta\mu/k_B T$ , the elastic assembly will grow faster; its shape becomes more distorted and ultimately buckles resulting in spikes growing out of the circle as shown in Fig. 1.

To study these morphological changes, we examine how the fluctuations of the elastic ring polymer are modified as a function of its growth rate. Specifically, we measure fluctuations in  $\hat{h}(x_n)$  where  $x_n \equiv n\langle l \rangle$ ,  $n$  labels the particles in the elastic ring and  $\hat{h}(x_n)$  denotes the deviation of the distance of a particle from the center of the assembly from the average radius of the elastic assembly,  $\hat{h}(x_n) \equiv h(x_n) - \langle h \rangle$ . The ensemble over which the fluctuations are measured was constructed by initiating simulations with a certain initial elastic assembly nucleus with size  $N_0$  and allowing the nucleus to grow for a time  $t_{\text{measure}}$ . In order to ensure that our results are not affected by choices of  $N_0$  and  $t_{\text{measure}}$ , simulations with multiple values of  $N_0$  and  $t_{\text{measure}}$  were considered. In ensembles constructed in this manner, we measured  $\langle |\delta h(q)|^2 \rangle$  where  $\delta h(q)$  is the Fourier transform of the radial fluctuations defined with the convention:  $\hat{h}(x_n) = \frac{1}{\sqrt{N}} \sum_q \delta h(q) \exp(iqx_n)$ ,  $q = \frac{2\pi m}{N\langle l \rangle}$ ,  $m = 1, 2, \dots, N$ . Here  $N$  is the number of particles in the elastic assembly.

At or close to equilibrium,  $\delta\mu/k_B T \ll 1$ , the radial fluctuations in our elastic ring can be characterized by an effective surface tension  $\gamma$  and a bending rigidity  $\kappa$ . Indeed in Fig. 2, we show that  $\langle |\delta h(q)|^2 \rangle$  scales like  $q^{-2}$

in the low frequency regime and scales like  $q^{-4}$  in the high frequency regime. This suggests that at equilibrium, the fluctuations of the elastic ring can be effectively described using the Helfrich Hamiltonian [30]:

$$E = \int \left\{ \frac{\gamma}{2} (\nabla \hat{h})^2 + \frac{\kappa}{2} (\Delta \hat{h})^2 \right\} dx \quad (2)$$

Even as the assembly starts to grow, Fig. 3 shows that the radial fluctuations are still described by an effective Helfrich Hamiltonian with renormalized surface tension and bending rigidities  $\gamma_{\text{eff}}$  and  $\kappa_{\text{eff}}$ . Indeed, Fig. 3 shows that the average  $\langle |\delta h(q)|^2 \rangle$  is well described by

$$\langle |\delta h(q)|^2 \rangle \propto \frac{k_B T}{(\gamma_{\text{eff}} q^2 + \kappa_{\text{eff}} q^4)}, \quad (3)$$

in accordance with Eq. 2. Closer inspection of the effective surface tension and bending rigidity extracted from Fig. 3 shows that the effective surface tension,  $\gamma_{\text{eff}}$  decreases as  $\delta\mu$  is increased, dropping to  $\gamma_{\text{eff}} \approx 0$  at a critical value of  $\delta\mu = \delta\mu_c$  (Fig. 4). Beyond this point, the elastic assembly buckles and undergoes a morphological transformation to ring populated by spikes. The number of spikes appearing in a process is proportional to the initial size of the assembly and  $\delta\mu$  (see Fig. 4) and remains constant during the growing period. Reflecting the diminished effective surface tension cost under non-equilibrium conditions, the configurations with spikes allow the system to grow with minimal penalties for stretching. The bending rigidity is also renormalized but by a smaller amount relative to the renormalization in the surface tension (Fig. SI 3). We again note that we performed numerical simulations with multiple initial sizes  $N_0$  and multiple choices of  $t_{\text{measure}}$ . The values of  $\delta\mu$ ,  $\gamma_{\text{eff}}$ ,  $\kappa_{\text{eff}}$ ,  $\delta\mu_c$  were independent of  $N_0$  and  $t_{\text{measure}}$  in our numerical simulations.

We now use ideas from stochastic thermodynamics to understand the trade-offs between non-equilibrium driving (as characterized by  $\delta\mu$ ) and morphological changes in the structure of this elastic ring system (as characterized by the renormalized constants  $\gamma_{\text{eff}}$  and  $\kappa_{\text{eff}}$ ). We begin by noting that our numerical results suggest that the even when the elastic ring is not at equilibrium, its fluctuations can be described in terms of an effective energy landscape, Eq. 3. In this case, the entropy of the growing elastic system at a time  $t$  can effectively be written down as [24, 32]

$$TS = \langle N \rangle_t \frac{-F_{\text{eff}} + \langle E_{\text{eff}} \rangle_N}{N}, \quad (4)$$

where  $E_{\text{eff}}$  is the effective elastic energy of a configuration in terms of the renormalized material parameters  $\gamma_{\text{eff}}$  and  $\kappa_{\text{eff}}$ ,  $F_{\text{eff}}$  is the Helmholtz free energy appropriate to  $E_{\text{eff}}$ ,  $\langle \dots \rangle_N$  is the average of all microscopic configurations of the assembly at size  $N \gg 1$  and  $\langle N \rangle_t$  is the average size of the elastic ring after it has been allowed to grow

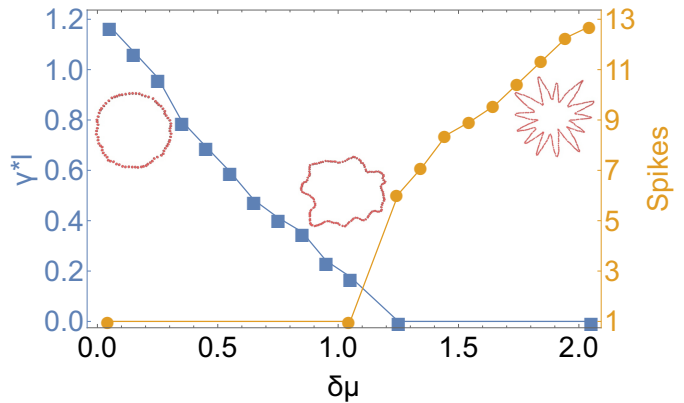


FIG. 4. Phase diagram for data at  $k_s = 4$  and  $k_\theta = 6$ . As  $\delta\mu$  is increased, the effective surface tension  $\gamma_{\text{eff}}$  decreases eventually reaching  $\gamma_{\text{eff}} \approx 0$  for  $\delta\mu \approx 1.0$ . Increasing  $\delta\mu$  beyond this value induces a morphological change to a configuration with spikes. The data was obtained with  $N_0 = 200$ .

for a time  $t$ . Since  $d\langle N \rangle_t / dt > 0$  under non-equilibrium conditions  $\delta\mu > 0$ , the entropy of the system changes as a function of time.

We can similarly compute the change in the entropy of the bath as it supplies monomers to the elastic assembly and maintains constant chemical potential conditions. Specifically, in the limit that the bath size is much larger than the size of any elastic assembly, the change in entropy of the bath after a time  $t$ ,  $\Delta S_{\text{bath}}$ , can be written as :

$$T\Delta S_{\text{bath}} = -\langle N \rangle_t \frac{-F_{\text{eq}} + \langle E_{\text{eq}} \rangle_N - N\delta\mu}{N} \quad (5)$$

By combining Eq. 4 and Eq. 5, we can write down the total entropy of the process, which must be nonnegative according to the second law of thermodynamics [32]:

$$\begin{aligned} \frac{dS_{\text{total}}}{dt} &= \frac{dS}{dt} + \frac{dS_{\text{bath}}}{dt} \\ &= \frac{d\langle N \rangle}{dt} (\delta\mu - \langle \epsilon_{\text{diss}} \rangle) \geq 0 \end{aligned} \quad (6)$$

Here  $\langle \epsilon_{\text{diss}} \rangle = (\langle E_{\text{eq}} - E_{\text{eff}} \rangle_N - (F_{\text{eq}} - F_{\text{eff}})) / N$ . For a growing system,  $\frac{d\langle N \rangle}{dt}$  is positive thus reducing the second law to:

$$\delta\mu - \langle \epsilon_{\text{diss}} \rangle \geq 0 \quad (7)$$

In addition, using the recently derived uncertainty relations that relate the entropy production to the current fluctuations of the system [9, 24, 33], we can propose a tighter phenomenological bound:

$$\delta\mu - \langle \epsilon_{\text{diss}} \rangle \geq \frac{vk_B T}{D} \quad (8)$$

where  $v = \frac{d\langle N \rangle}{dt}$  is the growth rate of the assembly, and  $D = \lim_{\tau \rightarrow \infty} \frac{\langle \Delta N^2 \rangle}{2\tau}$  is the diffusion constant of the size fluctuations of the assembly.

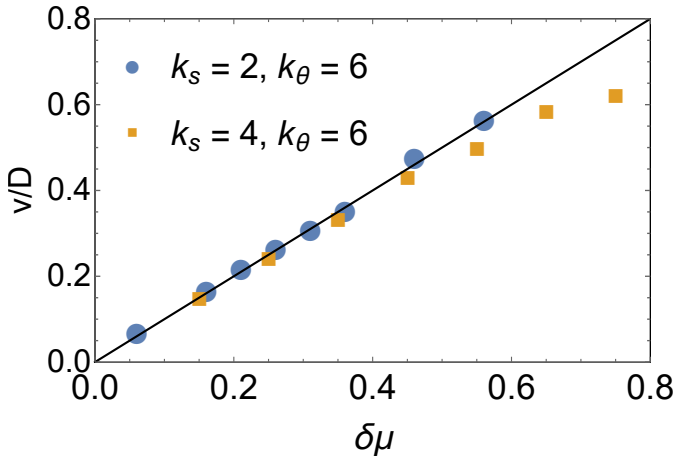


FIG. 5.  $\frac{v}{D}$  vs.  $\delta\mu$ . In this case,  $k_B T$  is set to 1. The dark line is predicted from linear response Eq. 9.

We note that the thermodynamic uncertainty relations have formally been derived for Markov processes on finite graphs while our system has no size constraints. Given that our numerical results suggest that the system settles into a steady state with system size independent elastic constants, we anticipate that there exists an effective Markov network with time independent rates that can mimic the time independent steady state behavior observed in our system. In the SI, we construct one such effective finite Markov state network. These numerical and phenomenological considerations allow us to propose the bounds in Eq. 7 and Eq. 8. These bounds constrain the allowed values of  $\gamma_{\text{eff}}$  and  $\kappa_{\text{eff}}$  given  $\delta\mu$ , the equilibrium elastic constants  $\gamma_{\text{eq}}, \kappa_{\text{eq}}$  and the ratio  $vk_B T/D$ .

In the limit of slow growth where the effective elastic constants are minimally renormalized,  $\delta\mu \gg \epsilon$ , Eq. 8 reduces to the following statement of linear response,

$$\delta\mu = \frac{vk_B T}{D} \quad (9)$$

In Fig. 5 we numerically verify that our simulations indeed satisfy this linear response condition, Eq. 9 when  $\delta\mu/k_B T \ll 1$ . Further, Fig. 5 also shows that  $\delta\mu \geq vk_B T/D$  in agreement with Eq. 8.

Motivated by these numerical results and the mapping constructed in the SI, we will now use Eq. 8 to understand how  $\gamma_{\text{eff}}$  can be controlled by tuning  $\delta\mu$ . As first approximation, given the relatively slow renormalization of the bending rigidity (Fig SI 3), we will set  $\kappa_{\text{eff}} = \kappa_{\text{eq}}$ . Within this approximation, an expression for  $\langle \epsilon_{\text{diss}} \rangle$  can be obtained as:

$$\langle \epsilon_{\text{diss}} \rangle = \frac{k_B T \lambda}{4\pi} \left( \frac{(\gamma + \gamma_{\text{eq}})\phi - 2\sqrt{\gamma\gamma_{\text{eq}}}\phi^*}{\sqrt{\gamma\kappa_{\text{eq}}}} - \frac{2\pi\xi}{\lambda} \right) \quad (10)$$

Here  $\phi = \arctan\left(\frac{2\pi\sqrt{\kappa_{\text{eq}}}}{\lambda\sqrt{\gamma}}\right)$ ,  $\phi^* = \arctan\left(\frac{2\pi\sqrt{\kappa_{\text{eq}}}}{\lambda\sqrt{\gamma_{\text{eq}}}}\right)$ ,  $\xi = \ln\left(\frac{\gamma_{\text{eq}}\lambda^2 + 4\pi^2\kappa_{\text{eq}}}{\gamma\lambda^2 + 4\pi^2\kappa_{\text{eq}}}\right)$ , and  $\lambda$  is the smallest wavelength al-

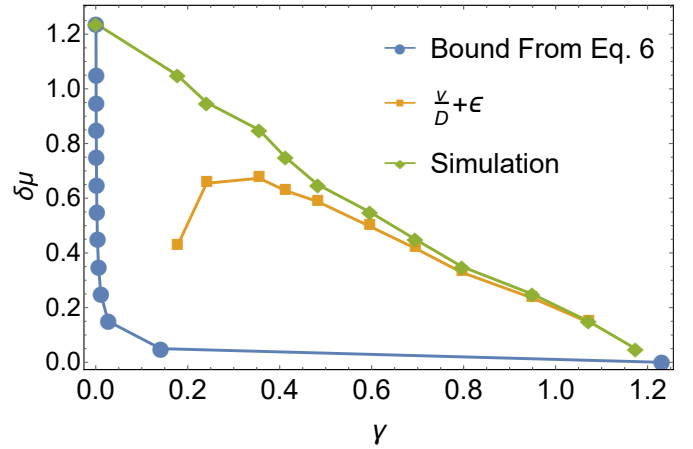


FIG. 6. Thermodynamic bounds on the surface tension as a function of the non-equilibrium driving force  $\delta\mu$ . The bound stipulated by the blue curve is from Eq. 7. The bound stipulated by the orange curve is from Eq. 8. The green curve is obtained by measuring  $\gamma_{\text{eff}}$  from simulations and is consistent with the bounds specified by Eq. 7 and Eq. 8. These bounds provide rough estimates for the energetic costs required to modify the morphology and fluctuations in the elastic membrane.

lowed by the assembly which we will take to be  $l_0$ . Using this expression for  $\epsilon_{\text{diss}}$ , Eq. 7 and Eq. 8 can be used to predict how  $\gamma_{\text{eff}}$  depends on the non-equilibrium driving  $\delta\mu$ . These predictions are plotted in Fig. 6 alongside the scaling of  $\gamma_{\text{eff}}$  with  $\delta\mu$  extracted from simulations.

The blue curve is obtained from the bound in Eq. (7), while the orange curve is from Eq. (8). The green curve was obtained from the simulations. As expected from linear response theory, the bound in Eq. 8 agrees very well with simulation results close to equilibrium. Away from equilibrium, Eq. 8 indeed provides a lower bound for  $\delta\mu$ . As we approach the instability  $\gamma_{\text{eff}} \approx 0$ , the predictive nature of the bound worsens and becomes saturated at the instability. We anticipate that a combination of finite size effects and large fluctuations close to the instability lead to the bound for  $\gamma_{\text{eff}}$  becoming unreliable closer to the instability. Despite these shortcomings, Fig. 6 shows how ideas from stochastic thermodynamics can be used to predict how material properties such as the surface tension, can be modified in the presence of non-equilibrium forces. It also provides a thermodynamic lower bound for the minimum non-equilibrium driving force  $\delta\mu$  required to obtain  $\gamma_{\text{eff}} \sim 0$  and induce morphological transformations in the system.

The role played by non-equilibrium forces in biological processes such as those responsible for modulating cell shapes and dynamics is well established [10–13, 16]. Using the formalism of stochastic thermodynamics, we have phenomenologically probed the tradeoffs between energy consumption and organization in a non-equilibrium growth process. Given the minimal kinetic

detail required by our effectively thermodynamic bounds, we anticipate that our results will find broad applicability in studies of the above mentioned non-equilibrium biophysical processes.

The authors acknowledge support from NSF DMR-MRSEC 1420709 and the University of Chicago. MN acknowledges support from the NSF GFRP. SV acknowledges support from the Sloan Fellowship.

- 
- [1] C. Battle, C. P. Broedersz, N. Fakhri, V. F. Geyer, J. Howard, C. F. Schmidt, and F. C. MacKintosh, *Science* **352**, 604 (2016).
- [2] G. Lan, P. Sartori, S. Neumann, V. Sourjik, and Y. Tu, *Nature physics* **8**, 422 (2012).
- [3] P. Mehta and D. J. Schwab, *Proceedings of the National Academy of Sciences* **109**, 17978 (2012).
- [4] S. Whitelam, L. O. Hedges, and J. D. Schmit, *Phys. Rev. Lett.* **112**, 155504 (2014).
- [5] J. J. Hopfield, *Proceedings of the National Academy of Sciences* **71**, 4135 (1974).
- [6] A. Murugan, D. A. Huse, and S. Leibler, *Proceedings of the National Academy of Sciences* **109**, 12034 (2012).
- [7] A. Murugan and S. Vaikuntanathan, *Journal of Statistical Physics* **162**, 1183 (2016).
- [8] A. Murugan and S. Vaikuntanathan, *Nature Communications* **8**, 13881 (2017).
- [9] A. C. Barato and U. Seifert, *Phys. Rev. Lett.* **114**, 158101 (2015).
- [10] H. T. McMahon and J. L. Gallop, *Nature* **438**, 590 (2005).
- [11] H. Turlier, D. A. Fedosov, B. Audoly, T. Auth, N. S. Gov, C. Sykes, J. F. Joanny, G. Gompper, and T. Betz, *Nature Physics* **12**, 513 (2016).
- [12] J. C. Stachowiak, E. M. Schmid, C. J. Ryan, H. S. Ann, D. Y. Sasaki, M. B. Sherman, P. L. Geissler, D. A. Fletcher, and C. C. Hayden, *Nature Cell Biology* **14**, 944 (2012).
- [13] Z. Chen, E. Atefi, and T. Baumgart, *Biophysical Journal* **111**, 1823 (2016).
- [14] P. Rangamani, K. K. Mandadap, and G. Oster, *Biophysical journal* **107**, 751 (2014).
- [15] S. Leibler, *Journal de Physique* **47**, 507 (1986).
- [16] K. Gowrishankar, S. Ghosh, S. Saha, C. Rumamol, S. Mayor, and M. Rao, *Cell* **149**, 1353 (2012).
- [17] J. Weichsel and P. L. Geissler, *PLoS computational biology* **12**, e1004982 (2016).
- [18] U. Seifert, *Reports on Progress in Physics* **75**, 126001 (2012).
- [19] C. Ganguly and D. Chaudhuri, *Physical Review E - Statistical, Nonlinear, and Soft Matter Physics* **88**, 1 (2013), arXiv:1304.7138.
- [20] C. del Junco, L. Tociu, and S. Vaikuntanathan, *ArXiv e-prints* (2016), arXiv:1611.00635 [cond-mat.soft].
- [21] K. Dasbiswas, K. K. Mandadapu, and S. Vaikuntanathan, arXiv preprint arXiv:1706.04526 (2017).
- [22] B. Gaveau, M. Moreau, and L. S. Schulman, *Physical Review Letters* **105**, 1 (2010).
- [23] U. Seifert, *Physical Review Letters* **106**, 1 (2011), arXiv:1011.2633.
- [24] M. Nguyen and S. Vaikuntanathan, *Proceedings of the National Academy of Sciences* **113**, 14231 (2016).
- [25] D. Drasdo, *Physical Review Letters* **84**, 4244 (2000), arXiv:0034180349.
- [26] S. Ramaswamy, J. Toner, and J. Prost, *Physical Review Letters* **84**, 3494 (2000), arXiv:9910022 [cond-mat].
- [27] M. Rao and R. C. Sarasij, *Physical Review Letters* **87**, 128101 (2001), arXiv:0009167 [cond-mat].
- [28] J. Solon, J. Pécréaux, P. Girard, M. C. Fauré, J. Prost, and P. Bassereau, *Physical Review Letters* **97**, 3 (2006).
- [29] E. Hannezo, J. Prost, and J. F. Joanny, *Physical Review Letters* **107**, 1 (2011), arXiv:1203.2080.
- [30] W. Helfrich, *Zeitschrift für Naturforschung Teil C Biochemie Biophysik Biologie Virologie* **28**, 693 (1973).
- [31] B. Loubet, U. Seifert, and M. A. Lomholt, *Physical Review E - Statistical, Nonlinear, and Soft Matter Physics* **85**, 1 (2012), arXiv:1112.2919.
- [32] M. Esposito, *Physical Review E - Statistical, Nonlinear, and Soft Matter Physics* **85**, 1 (2012), arXiv:1112.5410.
- [33] T. R. Gingrich, J. M. Horowitz, N. Perunov, and J. L. England, *Physical Review Letters* **116**, 120601 (2016).